24th INTERNATIONAL CONGRESS ON SOUND AND VIBRATION
23–27 July 2017, London

EXPERIMENTAL AND NUMERICAL INVESTIGATION OF RESONATOR BASED ACOUSTIC DAMPING

Felix Grimm, Michael Stöhr, Berthold Noll, Manfred Aigner
German Aerospace Center (DLR) - Institute of Combustion Technology, Stuttgart, Germany
email: felix.grimm@dlr.de

Jürgen Dierke, Roland Ewert
German Aerospace Center (DLR) - Institute of Aerodynamics and Flow Technology, Braunschweig, Germany

Combustion induced noise and thermoacoustic limit cycle phenomena significantly contribute to engine noise levels in civil aviation. Therefore, the development of reliable noise reduction strategies is a prevailing research field. In the presented paper, resonator based damping panels are experimentally and numerically investigated. The TNF standard DLR-A jet flame is studied with encasement and damping panels. Those acoustic liners are designed as an array of Helmholtz resonator similar elements. Therefore, a design strategy derived from a mechanical spring-mass-damper analogy is used. Frequency dependent impedance functions are evaluated with geometrical parameters of the acoustic liner. Three different configurations are tested for the damping panels: Sound hard walls, damping of the first acoustic longitudinal mode and the first acoustically stable transverse mode in the flame tube.
Experimental results are compared to numerical simulations with the Fast Random Particle Method for Combustion Noise Prediction (FRPM-CN). The approach relies on stochastic, particle based sound source reconstruction with turbulence statistics from CFD calculations. Sound propagation is computed via linearized Euler equations. Damping panels are simulated with an Extended Helmholtz Resonator (EHR) model, implemented in the PIANO research code.

Keywords: CFD, Computational Combustion Acoustics (CCA), FRPM-CN, EHR, Helmholtz-Resonator.

1. Introduction

Combustion noise and thermoacoustic instabilities are an increasingly important issue in modern, lean-premixed aero-engines and gas turbines. Especially in the field of aviation, noise emissions have become a widely recognized and investigated problem, due to more and more strict emissions regulations. The development of reliable noise and pressure oscillation damping techniques is therefore a highly relevant, topical research field. In the presented paper, resonator based damping mechanisms of resonance phenomena are addressed numerically and experimentally.
A key issue of the presented study is the theoretical assessment of damping mechanisms. In principle, there are two possibilities for the modelling of damping elements in time-domain [1]. A wide-spread method is the formulation of frequency-dependent multi-pole boundary conditions, where any customized impedance characteristics can be imposed [2], without the need for a direct depiction of physical effects. As a downside of this variant, impedance characteristics have to be known a priori from measurements. The second possibility is the direct modeling of physical effects via e.g. simple mass-spring-damper analogies, where damping characteristics can be determined based on only

few system parameters [3]. In this approach, the design of damping panels can be carried out based on fluid medium characteristics and geometric specifications of the resonators. On the other hand, relatively small time-steps have to be chosen for stability and modeling reasons. In fundamental investigations it can be nonetheless advantageous to choose a simplified representation of damping panels with all the same incorporation of physical mechanisms, in order to gain a more detailed understanding of damping processes. In the presented work therefore a physically motivated model is chosen.

The paper is structured as follows: First it is shown that the hybrid method FRPM-CN efficiently and reliably predicts resonance modes in the flame tube, not only in terms of frequency, but also for sound pressure amplitudes. Then, a design procedure for the EHR approach based on geometrical parameters of the liner configurations is used. Subsequently, parametric studies are carried out, identifying the impact of different damping system components like resonator volume, viscous damping, or flow resistance on resulting sound pressure spectra. Based on this, an optimized simulation with the EHR model is compared to the measured damping configurations. It is shown that FRPM-CN in combination with the EHR approach accurately reproduces damping effects of the presented experiment.

2. The *Extended Helmholtz Resonator* (EHR) Model

Impedance as an aggregation of acoustic damping mechanisms has complex valued properties. It can be described by the simple relation

$$Z(i\omega) = X(\omega) + iY(\omega). \tag{1}$$

The real part of Z, X, is called resistance, while the imaginary fraction Y stands for reactance [4]. $\omega = 2\pi f$ is the angular frequency. Acoustic resistance describes energy transfer between acoustic waves and the surrounding media, mainly by a turnover of heat. Reactance comprises phenomena of momentum exchange and elasticity. For the frequency dependent description of damping device characteristics, coefficients for absorption and reflection are employed, evaluated by

$$\alpha_Z(\omega) = 1 - |R_Z(\omega)|^2 = 1 - \left|\frac{Z(\omega) - Z_0}{Z(\omega) + Z_0}\right|^2, \tag{2}$$

with the sound impulse impedance $Z_0 = \rho_0 c_0$, where ρ_0 and c_0 are density and speed of sound of the fluid medium.

For the numerical simulations realizing frequency dependent impedance like in Eq. (1) for damping devices, an *Extended Helmholtz Resonator* (EHR) model as introduced by Rienstra [3] is employed in this work. We make us of an implementation in the PIANO research code from Bassetti et al. [5, 6] with the theoretical description of the model from Richter et al. [7, 8]. It is used in combination with 2D FRPM-CN, the Fast Random Particle Method for Combustion Noise prediction [9]. The EHR model was derived based on an analogy to a mechanical spring-mass-damper system, as schematically shown in Fig. 1. In general, frequency dependent impedance of such a spring-mass-damper system can be generally expressed by

$$Z(i\omega) = \frac{\hat{p}}{\hat{u}_n} = i\omega m_m + d + \frac{k_m}{i\omega}, \tag{3}$$

with the area related quantities m_m, k_m and d for element mass M_m, spring constant K_m and damping devices D in Fig. 1. $\hat{p}$ and $\hat{u}_n$ are harmonized pressure and sound speed. The equivalent to the mechanical system is the so called Helmholtz resonator, as sketched in Fig. 1 (right). Extensive theoretical background and description can be found in the literature [10, 8]. In practical applications, damping devices consist of multiple Helmholtz resonators aligned in arrays. The design strategy for such panels [11] often makes use of the ratio of active or effective area (open area) to overall panel

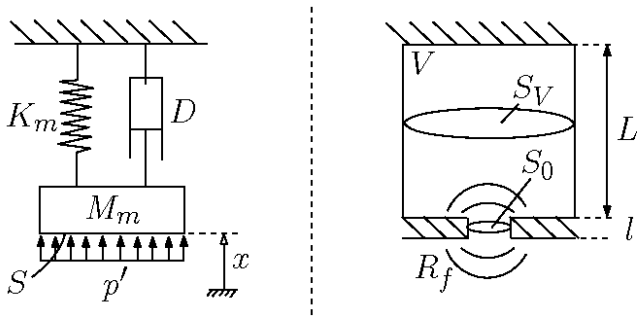

Figure 1: Mechanical spring-mass-damper analogy (left) and Helmholtz resonator (right) [8].

area, the so called porosity $\sigma = S_0/S$. As a consequence, resonator frequency, mass and damping constant amount to

$$m_m = \frac{\rho_0 L}{\sigma} \quad \text{and} \quad k_m = \frac{S\rho_0 c^2}{V} \quad \text{and} \quad \omega_0 = \sqrt{\frac{\sigma S c^2}{VL}}. \tag{4}$$

Corresponding geometrical quantities are given according to Fig. 1. S_0 is the neck hole cross-section of the resonator neck, L denotes the length of the resonator, while V are the cavity volume and ρ_0 the fluid density in the device. The frequency dependent impedance of the EHR model is [8]

$$Z_{\text{EHR}}(i\omega) = i\omega m_f + R_f - i\beta \cot\left(\frac{\omega T_l}{2} - i\frac{\epsilon}{2}\right). \tag{5}$$

R_f represents the real-valued resistance of the front plate with viscous and vortex-induced effects. m_f symbolizes mass inertia in resonator neck and volume. β denotes a reactance parameter in the resonator cavity. T_l describes a time-delay induced by the panel geometry and abstracts essentially the dynamic behavior of sound waves on their way through the resonator. ϵ stands for damping of the fluid in the cavity. The PIANO code works in time-domain and therefore a corresponding formulation of the model is implemented as [5, 6]

$$\begin{aligned} p'(t) - e^{-\epsilon}(t - T_l) = (R_f + \beta)u_n'(t) - (R_f - \beta)e^{-\epsilon} \cdot u_n'(t - T_l) + \\ + m_f \left(\frac{\partial u_n'(t)}{\partial t} - e^{-\epsilon}\frac{\partial u_n'(t)}{\partial t}(t - T_l)\right). \end{aligned} \tag{6}$$

3. Resonator array design and experimental setup

The impedance characteristics of the damping panels are designed with the relation [12, 13]

$$Z_{\text{Liner}}(i\omega) = R + i\omega m + \frac{\rho c^2}{i\omega d}. \tag{7}$$

d stands for the distance of center axes of holes. A regular hole alignment as shown in Fig. 2 is considered. a is the radius of circular holes, l is the thickness of the damping panel front plate and L denotes the distance from front- to back-plate. For the flow resistance R and the mass in the neck section of the damping devices m

$$R = R_0 + 2\Delta R \quad \text{and} \quad m = \frac{\rho}{\sigma}(l_0 + 2\Delta l) \tag{8}$$

is applied. The area ratio of the acoustic lining of effective, active area $S = \pi a^2$ to overall area $S = d^2$, describes the porosity of the damping panel, $\sigma = \pi a^2/d^2$. Interactions of resonator elements are neglected and it is assumed that an equivalent volume behind the perforated plate is associated to

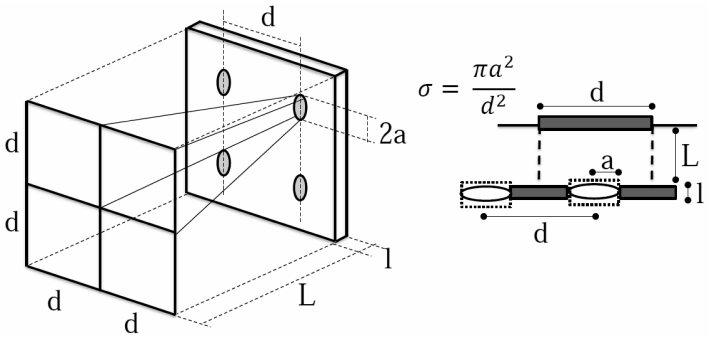

Figure 2: Schematic drawing of measured damping panel and area ratio of perforated and back plate [12].

each resonator element, as indicated in Fig. 2. A correction for the oscillating mass in the resonator necks is applied [14, 12],

$$\Delta l = 0.8a(1 - 1.4\sqrt{\sigma}). \tag{9}$$

Equation (9) takes into account the interaction of the single holes in the range of $\sigma \leq 0.2$. The flow resistance R in Eq. (8) contains a fraction for the viscous resistance in the resonator neck R_0 and the viscous resistance at hole edges via motion of the fluid medium $2\Delta R$ in the regions outside of the neck. Whether the neck area is narrow or wide in terms of viscous damping, a so called viscous wave length [12] $\lambda_\eta = 0.0137/\sqrt{f}[m]$ is defined. This criterion is explicitly applied for each frequency in the resonator design process. Above a threshold value $a \geq 0.63\lambda_\eta$, a wide opening is defined and below the value, a narrow opening is considered,

$$R_{0,W} = 0.53 \cdot 10^{-2} \frac{d^2 l}{a^3} \sqrt{f} \left[\frac{Ns}{m^3}\right] \text{ or } R_{0,N} = 0.46 \cdot 10^{-4} \frac{d^2 l}{a^4} \left[\frac{Ns}{m^3}\right]. \tag{10}$$

In both cases, the correction $2\Delta R$ is evaluated with

$$2\Delta R = 1.05 \cdot 10^{-2} \frac{d^2}{a^2} \sqrt{f} \left[\frac{Ns}{m^3}\right]. \tag{11}$$

The experimental setting is shown in Fig. 3. Two different damping configurations are tested, lined walls with resonator elements and lined walls without back plate ($L \to \infty$). Accompanying this, pressure spectra for sound hard walls are measured, as in preceding studies [15]. In the case of lined walls, a constant radial distance between perforate and solid wall is ensured via set screws. For manufacturing reasons, perforated walls are commercially available plates, therefore the design parameters of plate thickness l, hole distance d and hole radius a are strongly limited. The parameter to be mainly varied in relevant regions is the radial length L, determining the resonator volumes. It is however limited through the assumption of a locally plane damping panel, which is implied in the design process as previously introduced. It can be shown with parametric studies that an increase in resonator volume by increasing L, lower frequencies are damped. For the design point $f_2 = 1600Hz$, as shown in Fig. 3, the parameters $L = 0.0065m, l = 0.002m, a = 0.00225m, d = 0.025m$ and $\sigma = 0.03$ are realized in experiments and $L \to \infty$ for the treatment of $f_2 = 260Hz$. The panel design procedure is carried out for ambient air conditions.

The flame tube has an inner diameter of $37.5d/D$ and a length of $62.5y/D$ and is mounted to a horizontally aligned base plate. Acoustic pressure recorders are mounted concisely with the perforated wall with positions as shown in Fig. 3. The upstream fuel inlet tube has the diameter $D = 0.008m$, which is used for referencing purposes and a length of $43.75y/D$. Brül& Kjaer type 4939 microphones are used with a type 2670 preamplifier. Measurements are carried out at $p_\infty = 957.7hPa$. Time samples are collected with a sampling rate of 200kHz, while resulting pressure spectra are evaluated over a time span of 60s and a narrow band spectrum with $\Delta f = 1Hz$ is evaluated.

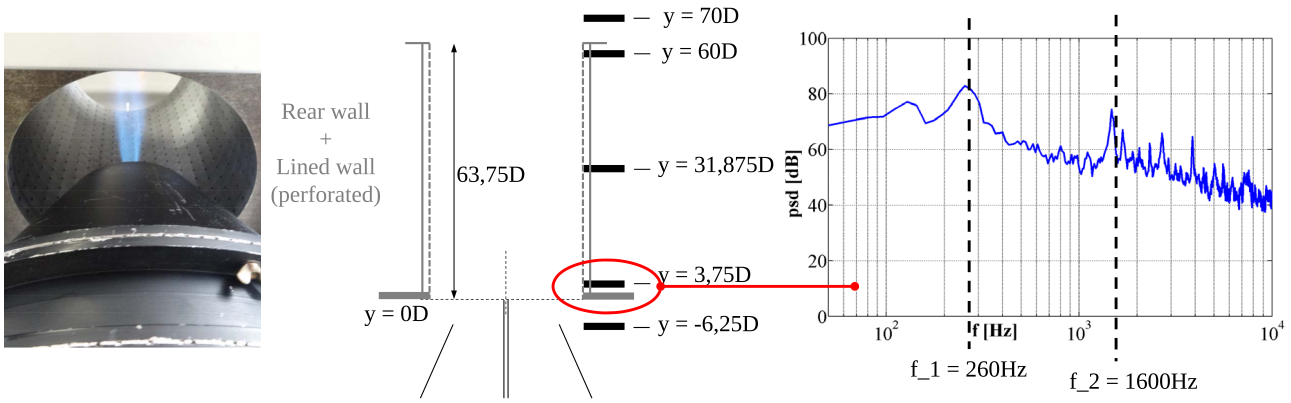

Figure 3: Experimental setup with the damping panel at operation (left), basic test rig dimensions with measurement positions (middle), and measured acoustic pressure spectrum with sound hard walls and the two considered design points for the damping panels (right).

The test rig is operated at atmospheric conditions with a fuel composition of 22.1 Vol-% CH_4, 33.2 Vol-% H_2, and 44.7 Vol-% N_2 and a stoichiometric mixture fraction of $f_Z = 0.167$. The jet flame is surrounded by a coflow emerging from an exit diameter of $17.5d/D$. Applied mass flow rates are $\dot{m}_{\mathrm{CH4}} = 18.02g/min$, $\dot{m}_{\mathrm{N2}} = 3.4g/min$, $\dot{m}_{\mathrm{H2}} = 63.65g/min$, and for air and coflow combined, $\dot{m}_{\mathrm{air}} = 320.64g/min$, yielding a Reynolds number of about 15200.

4. Numerical Setup

Prior to the combustion acoustics simulations, steady state, reacting CFD simulations are carried out [15]. Therefrom obtained mean flow field and combustion quantities serve as background flow field for the acoustics simulations. Integral turbulence statistics from the CFD simulations are taken as input for stochastic sound source reconstruction with FRPM-CN, the Fast Random Particle Method for Combustion Noise Prediction. Sound propagation is modeled with linearized Euler equations. The numerical setup for the combustion acoustics simulations of the encased DLR-A flame with damping panels is depicted in Fig. 4. The technical specifications of the setup shown in Fig. 4 can be found in

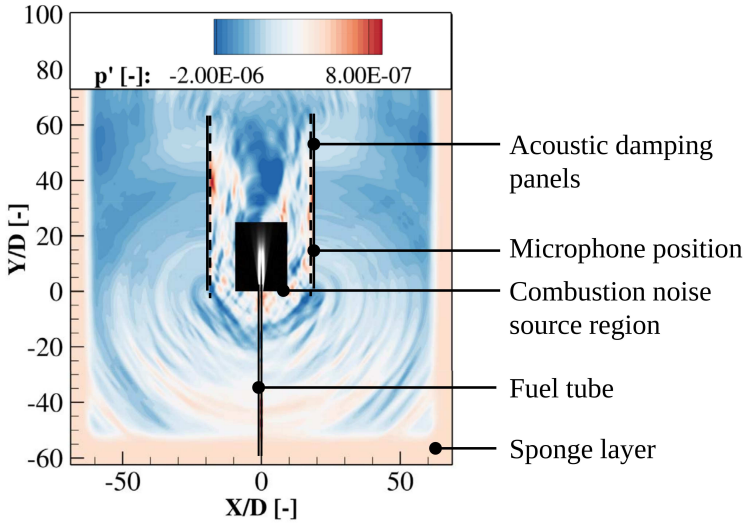

Figure 4: Setup of the computational combustion acoustic simulations with FRPM-CN and damping panels with instantaneous acoustic pressure field solution, combustion noise source field location and indicated pressure recorder position.

the literature [9]. Additionally, sound hard walls or EHR (Extended Helmholtz Resonator) boundary conditions are set accordingly to the experimental configuration.
EHR boundary conditions have to be adjusted, in order to display a frequency dependent absorption coefficient as a function of complex valued impedance. Several model parameters have to be defined, according to Eqs. (5) and (6). The EHR model requires five input parameters, while three of them can be estimated from geometric relations. The following constrictions [16, 8] hold for causality reasons,

$$R_f \geq 0,\ m_f \geq 0,\ T_l \geq 0,\ \beta \geq 0,\ \text{and}\ \epsilon \geq 0. \tag{12}$$

A first estimate of the EHR model parameters is carried out with [8]

$$T_l = \frac{2}{f_0},\quad \beta = \frac{c\sigma}{L}\frac{T_l}{2},\quad \text{and}\quad m_f = \frac{L}{\sigma}(1+2\Delta l) - \frac{c^2\sigma}{L}\frac{T_l^2}{12}. \tag{13}$$

Furthermore,

$$\frac{S}{V} = \frac{1}{c}\frac{2\beta T_l}{T_l^2 + \frac{\epsilon^2}{\omega^2}}. \tag{14}$$

c denotes the local speed of sound and f_0 is the target resonance frequency. ϵ is determined empirically, while causality has to be kept. For preliminary design, the relation $L/\sigma = m_f + c\beta T_l/6$ can be taken into account. R_f is evaluated from Eq. (8). However by using the previously introduced system of equations for calibration of the numerical model, inconsistency in view of the causality conditions (Eq. (12)) is likely to appear. In order to study parametric sensitivity, a parametric space as shown in Table 1 is covered in several simulation runs. A total simulation time of $t = 0.2s$ is computed with resulting 200k discrete time samples respectively for evaluation of sound pressure spectra.

Table 1: Operating point dependent dimensionless parametric space investigated for EHR model calibration.

f_1	**Parametric range**	f_2	**Parametric range**
260Hz	$R_f \in [0.0025; 0.04]$	1600Hz	$R_f \in [0.003; 0.1]$
	$m_f \in [0.02; 0.67]$		$m_f \in [0.02; 0.68]$
	$T_l \in [0.17; 5.4]$		$T_l \in [0.028; 0.91]$
	$\beta \in [0; 0.5]$		$\beta \in [0; 0.5]$
	$\epsilon \in [0; 0.4]$		$\epsilon \in [0; 0.4]$

5. Results

Experimental and simulation results are shown in Fig. 5 for damping of both design points $f_1 = 260Hz$ and $f_2 = 1600Hz$ and the sound hard wall configuration. Sound pressure spectra of measurements of design points for damped resonances at design frequencies $f_1 = 260Hz$ and $f_2 = 1600Hz$ and configurations with sound hard walls are shown in Figs. 5(a) and (c). Mainly low frequencies are damped in the case of perforated plate without back plate for f_1 (a), however acoustic damping is in this case also present for the transverse mode at f_2. For the lined case in Fig. 5(c), only the target frequency range around $f_2 = 1600Hz$ is damped compared to the sound hard wall measurements. Due to affection of the first transverse mode by both damping configurations it is assumed that this resonance mode is damped by mainly viscous effects in the resonator neck.
CFD simulations are carried out with Ansys CFX 11 on two IBM Power 5 processors in 11 CPU-h [15]. One consecutive simulation with 2D FRPM-CN and the EHR model is conducted with PIANO 5.5 on a single Intel Yeon E31225 processor in about 10 CPU-h. The EHR simulation parameter sets for the respective resonance frequencies, evaluated from the parametric space shown in Table 1 are listed in Table 2. Parameters for flow resistance R_f and the neck mass m_f are in the same order

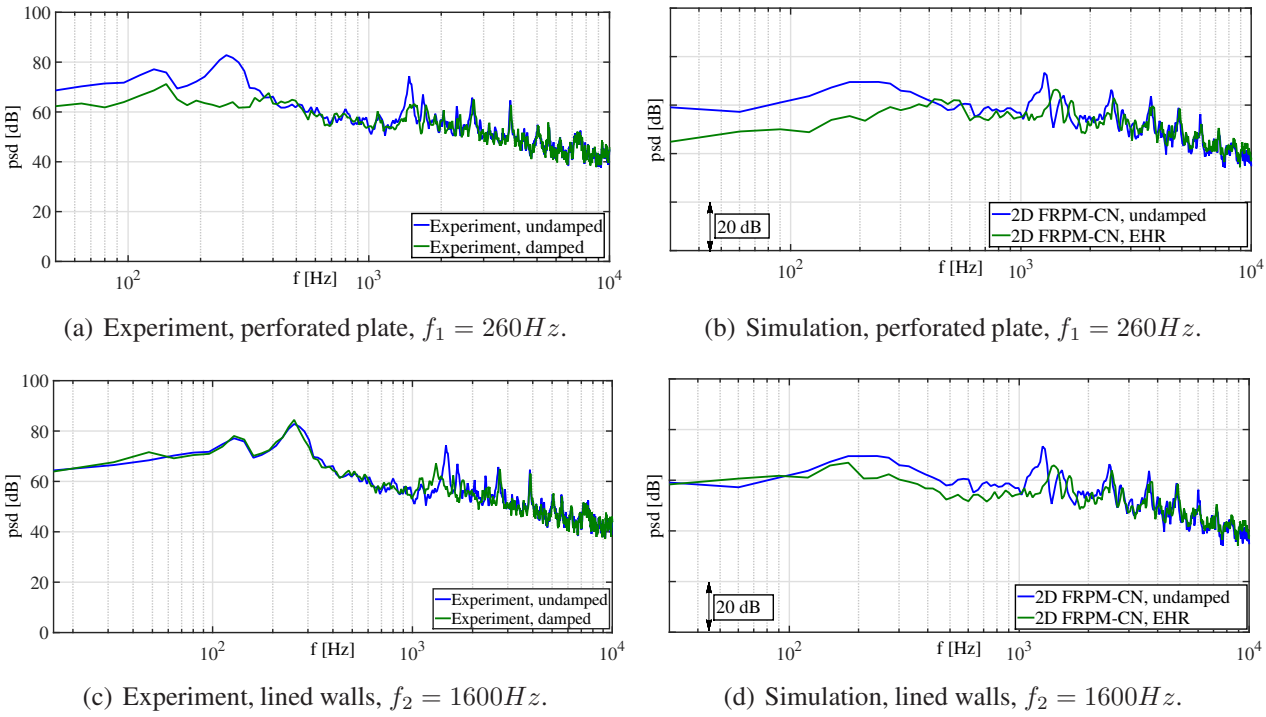

(a) Experiment, perforated plate, $f_1 = 260Hz$.

(b) Simulation, perforated plate, $f_1 = 260Hz$.

(c) Experiment, lined walls, $f_2 = 1600Hz$.

(d) Simulation, lined walls, $f_2 = 1600Hz$.

Figure 5: Comparison of sound pressure spectra from experimental data and results simulated with 2D FRPM-CN and EHR boundary condition for both design points $f_1 = 260Hz$ and $f_2 = 1600Hz$ and sound hard walls.

of magnitude for both design points, as expected from the experimental configuration. The time-delay parameter T_l is significantly larger for the configuration "perforated plate without back wall", in agreement with the experimental configuration. Furthermore, for the design point $f_1 = 260Hz$, β and ϵ, the parameters for resonator volume related damping, tend to zero for the case f_1, where no resonator volume effectively acts.

Table 2: Parameter set for simulation results in Fig. 5.

f_0	R_f	m_f	T_l	β	ϵ
260Hz	0.00508	0.084	2.707	0.01	0
1600Hz	0.0124	0.08493	0.11351	0.5	0.2

Resonance modes of the experiment in the tube are captured well by the numerical model in terms of frequency and magnitude. Deviations are present for the first peak at $f = 260Hz$, which is assigned to a longitudinal oscillation. By comparison of numerical simulations with sound hard walls and EHR boundary conditions it is found that effects of damping from the experiment are accurately reproduced for both design points, f_1 and f_2. However, relative trends are evaluated in the simulation results, since the numerical setup considers plane source modeling and sound propagation only.

6. Conclusions

Acoustic damping of resonance phenomena in an encased DLR-A jet flame configuration was studied experimentally and numerically. The design procedure of Helmholtz-resonator-similar arrays of damping panels was taken from architectural acoustics methods. Experimental results were found to be in good agreement with previously defined damping design points. The numerical model was able to reliably reproduce resonance modes in the flame tube for a large range of frequencies. Damping configurations were simulated with an Extended Helmholtz Resonator based model. Effects of acoustic damping were accurately captured by the numerical model.

Acknowledgments

This collaborative work was supported within the project DECISIVE which was funded by the German Aerospace Center (DLR).

References

1. Richter, C. A review of time domain impedance boundary conditions. societe francaise d'acoustique., *Proceedings of the Acoustics 2012 Nantes Conference*, nantes, France. hal-00810672, (2012).

2. Lourier, J.-M., Noll, B. and Aigner, M. Large eddy simulation of a thermoacoustic instability within a swirl-stabilized burner using impedance boundary conditions, *Proceedings of ASME Turbo Expo 2014*, gT2014-26200, (2014).

3. Rienstra, S. Impedance models in time domain including the extended helmholtz resonator model, *12th AIAA/CEAS Aeroacoustics Conference, Cambridge, MA, USA*, (2006).

4. Bellucci, V., Flohr, P. and Paschereit, C. Numerical and experimental study of acoustic damping generated by perforated screens, *AIAA Journal*, **42** (8), 1543–1549, (2004).

5. Bassetti, A., Guerin, S. and Kornow, O. Introducing lined-wall boundary conditions in the dlr time-domain caa solver piano, *DAGA Conference*, paper no. 160, (2010).

6. Bassetti, A., Guerin, S. and Busse, S. Validation of the caa solver piano with lined-wall boundary condition, *DAGA Conference*, paper no. 179, (2011).

7. Richter, C., Thiele, F., Li, X. and Zhuang, M. Comparison of time-domain impedance boundary conditions for lined duct flows, *AIAA Journal*, **45** (6), 1333–1345, (2007).

8. Richter, C., *Liner impedance modeling in the time domain with flow*, PhD Thesis, Technische Universität Berlin, https://opus4.kobv.de/opus4-tuberlin/frontdoor/index/index/docId/2408, (2009).

9. Grimm, F., Ewert, R., Dierke, J., Noll, B. and Aigner, M. The fast random particle method for combustion noise prediction, *20th AIAA/CEAS Aeroacoustics Conference*, aIAA Paper 2014-2451, (2014).

10. Ehrenfried, K., *Strömungsakustik*, Mensch und Buch Verlag AG, Berlin, ISBN 3-89820-699-8 (2004).

11. Fuchs, H., *Schallabsorber und Schalldämpfer*, Springer, Berlin, Heidelberg, ISBN 3-540-35493-X (2004).

12. Bräuer, J. and Weselak, W. Lochplatten-, schlitzplatten- und helmholtz-absorber, *Projektarbeit, Instistut für Breitbandkommunikation, TU Graz*, (2010).

13. Maa, D.-Y. Theory and design of microperforated panel sound absorbing constructions (chinesisch), *Scientia Sinica*, **18**, 55–71, (1975).

14. Ingard, U. On the theory and design of acoustic resonators, *J. Acoust. Soc. Am.*, **25**, 1037, (1953).

15. Mühlbauer, B., Stöhr, M., Noll, B. and Aigner, M. Broadband Combustion Noise Measurements and Numerical Simulation of Enclosed Turbulent Non-Premixed Jet Flames, *18th International Congress on Sound and Vibration*, rio de Janeiro, Brazil, (2011).

16. Chevaugeon, N., Remacle, J.-F. and Gallez, X. Discontinuous galerkin implementation of the extended helmholtz resonator model in time domain, *12th AIAA/CEAS Aeroacoustics Conference (27th Aeroacoustics Conference)*, aIAA 2006-2569, (2006).